
This is an electronic reprint of the original article.
This reprint may differ from the original in pagination and typographic detail.

Asghar, Imran; Lepikko, Sakari; Patakangas, Janne; Halme, Janne; Lund, Peter D.

Comparative analysis of ceramic-carbonate nanocomposite fuel cells using composite GDC/NLC electrolyte with different perovskite structured cathode materials

Published in:
Frontiers of Chemical Science and Engineering

DOI:
[10.1007/s11705-017-1642-2](https://doi.org/10.1007/s11705-017-1642-2)

Published: 01/01/2018

Document Version
Peer-reviewed accepted author manuscript, also known as Final accepted manuscript or Post-print

Please cite the original version:
Asghar, I., Lepikko, S., Patakangas, J., Halme, J., & Lund, P. D. (2018). Comparative analysis of ceramic-carbonate nanocomposite fuel cells using composite GDC/NLC electrolyte with different perovskite structured cathode materials. *Frontiers of Chemical Science and Engineering*, 12(1), 162–173.
<https://doi.org/10.1007/s11705-017-1642-2>

This material is protected by copyright and other intellectual property rights, and duplication or sale of all or part of any of the repository collections is not permitted, except that material may be duplicated by you for your research use or educational purposes in electronic or print form. You must obtain permission for any other use. Electronic or print copies may not be offered, whether for sale or otherwise to anyone who is not an authorised user.

Comparative analysis of ceramic-carbonate nanocomposite fuel cells using composite GDC/ NLC electrolyte with different perovskite structured cathode materials

Authors: M. I. Asghar¹, S. Lepikko¹, J. Patakangas¹, J. Halme¹, P. D. Lund¹

1) New Energy Technologies Group, Department of Applied Physics, Aalto University, P.O. BOX 15100, FIN-00076 Aalto, Finland

Corresponding author: Dr. Muhammad Imran Asghar
imran.asghar@aalto.fi

Key words: electrode, fuel cell, low-temperature, nanocomposite, perovskite

Abstract:

A comparative analysis of perovskite structured cathode materials, $\text{La}_{0.65}\text{Sr}_{0.35}\text{MnO}_3$ (LSM), $\text{La}_{0.8}\text{Sr}_{0.2}\text{CoO}_3$ (LSC), $\text{La}_{0.6}\text{Sr}_{0.4}\text{FeO}_3$ (LSF) and $\text{La}_{0.6}\text{Sr}_{0.4}\text{Co}_{0.2}\text{Fe}_{0.8}\text{O}_3$ (LSCF), was performed for a ceramic-carbonate nanocomposite fuel cell using composite electrolyte consisting of $\text{Gd}_{0.1}\text{Ce}_{0.9}\text{O}_{1.95}$ (GDC) and a eutectic mixture of Na_2CO_3 (NC) and Li_2CO_3 (LC). The compatibility of these nanocomposite electrode powder materials was investigated under air, CO_2 and air/ CO_2 atmospheres at 550°C . Microscopy measurements together with energy dispersive X-ray spectroscopy (EDS) elementary analysis revealed few spots with higher counts of manganese relative to lanthanum and strontium under pure CO_2 atmosphere. Furthermore, electrochemical impedance (EIS) analysis showed that LSC had the lowest resistance to oxygen reduction reaction (ORR) ($14.12 \Omega \text{ cm}^2$) followed by LSF ($15.23 \Omega \text{ cm}^2$), LSCF ($19.38 \Omega \text{ cm}^2$) and LSM ($>300 \Omega \text{ cm}^2$). In addition, low frequency EIS measurements (down to $50 \mu\text{Hz}$) revealed two additional semi-circles at frequencies below around 1 Hz. These semicircles can yield additional information about electrochemical reactions in the device. Finally, a fuel cell was fabricated using GDC/NLC nanocomposite electrolyte and its composite with NiO and LSCF as anode and cathode, respectively. The cell produced an excellent power density of 1.06 W/cm^2 at 550°C under fuel cell conditions.

1. Introduction

Nanocomposite low temperature solid oxide fuel cells (LT-SOFC; also referred as intermediate temperature hybrid fuel cells [1]), are emerging as a potential fuel cell technology. The motivation for this fuel cell technology originates from the fact that a solid oxide fuel cell (SOFC), a high efficiency fuel cell, operates at high temperatures between 800 °C and 1000 °C primarily due to a limited oxygen ion conductivity of yttria-stabilized zirconia (YSZ) which is used as an electrolyte material [2,3,4]. Such a high operating temperature leads to many degradation issues including chemical and mechanical incompatibilities, permanent microstructural changes and sealing issues [5-7]. To overcome this problem, alternative electrolyte materials such as gadolinium doped cerium oxide (GDC) and samarium doped cerium oxide (SDC) have been investigated to be used at lower temperatures (400°C – 600°C) to replace the YSZ based electrolyte [8-11]. Although their ionic conductivity (0.1 S/cm at 800°C) is much better than that of YSZ (0.1 S/cm at 1000°C) [12], their ionic conductivity can be further improved for lower temperatures (400°C – 600°C). There are two main approaches to improve the oxygen ion conduction through GDC or SDC electrolyte. One approach is to dramatically decrease the thickness of the electrolyte layer down to less than ten micrometer thickness [13]. The other approach is to utilize a nanocomposite electrolyte consisting of GDC/SDC and a eutectic mixture of alkali (Na, Li, K) carbonates [14-19]. The nanocomposite electrolytes significantly improve the ion conduction through the composite electrolyte even at low temperatures of around 500 °C. Depending on the composition of the nanocomposite electrolyte, the operating temperature could be reduced even down to 400 °C while keeping high enough ionic conductivity of the electrolyte [8].

Although molten carbonates improve the performance of the composite electrolytes, the carbonates can also corrode electrode materials. An XRD study has shown that strontium, which is a common element in potential perovskite structured cathode materials [20] including $\text{La}_{0.65}\text{Sr}_{0.35}\text{MnO}_3$ (LSM), $\text{La}_{0.8}\text{Sr}_{0.2}\text{CoO}_3$ (LSC), $\text{La}_{0.6}\text{Sr}_{0.4}\text{FeO}_3$ (LSF) and $\text{La}_{0.6}\text{Sr}_{0.4}\text{Co}_{0.2}\text{Fe}_{0.8}\text{O}_3$ (LSCF), can react with molten carbonates to form strontium carbonate [15]. However, it is not clear how detrimental these interactions are to the overall device performance and stability, since the intensity of the XRD peaks [15] were very low. It has been also reported that some of the potential perovskite structured electrode material,

LSM, degraded due to a reaction with manganese and molten carbonates [14]. Furthermore, it has also been reported that lithiated nickel oxide, which can be used as a cathode material, can also dissolve into the molten carbonate [1,21,22]. Therefore, a comparative compatibility study using the aforementioned electrode materials with nanocomposite electrolytes was carried out to identify potential electrode candidates. In addition, it is important to compare the performance of the potential electrode materials at low temperature operating conditions (400°C – 600°C) to identify their feasibility for LT-SOFC using nanocomposite electrolyte. As the potential perovskite structured cathode materials (LSM, LSC, LSF and LSCF) have different electrical conductivities (200-300 S/cm at 900°C [23], 1650 S/cm at 800°C [24], 350 S/cm at 550°C [20], ~230 S/cm at 900°C [20]) and ionic conductivities (10^{-7} S/cm at 900°C [23,25], 1.2 S/cm at 900°C [26], 1.2×10^{-5} S/cm at 700°C [27], 0.2 S/cm at 900°C [26]) respectively, which can result in different electrochemical performance. Though their thermal expansion coefficients (TEC) relative to other components in the cells can play a critical role for the long term stability of (high temperature) SOFC [28], their mismatch with other components has less crucial significance for lower operating temperatures of LT-SOFC.

In this work, four perovskite structured cathode materials, LSM, LSC, LSF and LSCF, were mixed with Na_2CO_3 (NC) and Li_2CO_3 (LC), and their performance as cathodes was compared. Compatibility tests were carried out at 550 °C under air, CO_2 and air/ CO_2 atmospheres, and the materials were analysed using X-ray diffraction (XRD), transmission electron microscopy (TEM) and energy dispersive X-ray spectroscopy (EDS). Additionally, symmetric cells were prepared using the above-mentioned nanocomposite cathode materials and were then characterized using electrochemical impedance spectroscopy (EIS), cyclic voltammetry (CV), scanning electron microscopy (SEM) and EDS. Finally, a complete fuel cell was fabricated and characterized in fuel cell operating conditions. This work provides a deeper insight into the mechanisms in the nanocomposite LT-SOFC and gives recommendations for more reliable electrode studies.

2. Experimental section

Materials

Except for LSM powder that was received from CSIR (Central Glass & Ceramic Research Institute), all the other powders, that is GDC, NC, LC, LSC, LSF, LSCF, NiO, polyvinyl-alcohol and ethyl-cellulose were purchased from Sigma Aldrich. Mixing of the materials was done in each step in a planetary ball mill at 60 rpm for 1 hour. Firstly, a mixture of NC (57 wt%) and LC (43 wt%) was prepared (abbreviated as NLC). Nanocomposite electrolyte powders were prepared by mixing GDC (87.8 wt%) and NLC (12.2 wt%) powders. Similarly, four different nanocomposite electrode powders were obtained by mixing LSM (50 wt%), LSC (50 wt%), LSF (50 wt%) and LSCF (50 wt%) with NLC (50 wt%), respectively.

Symmetric cells (electrode / electrolyte / electrode) were prepared by a co-pressing method by placing powders sequentially into a 13 mm die. A small pressure was applied each time a new layer was added. In the end, the cells were pressed under 250 MPa for 2 minutes to form 4 pellets with the different electrode materials but with the same electrolyte material. After that, the pellets were sintered at 690 °C for 30 min with the heating rate being 2 °C/min. The structure of each cell is shown in Table 1.

Table 1: The structure of the symmetric cells prepared by the co-pressing method.

Symmetric cells	
1.	LSM + NLC / GDC + NLC / LSM + NLC
2.	LSC + NLC / GDC + NLC / LSC + NLC
3.	LSF + NLC / GDC + NLC / LSF + NLC
4.	LSCF + NLC / GDC + NLC / LSCF + NLC

In addition, the compatibility of the composite electrode materials under air, CO₂ and air/CO₂ (50 vol% / 50 vol%) atmospheres was tested by exposing the samples to the

aforementioned gas atmospheres in an oven at 550°C for 5 hours. The setup of the oven is shown in Figure 1.

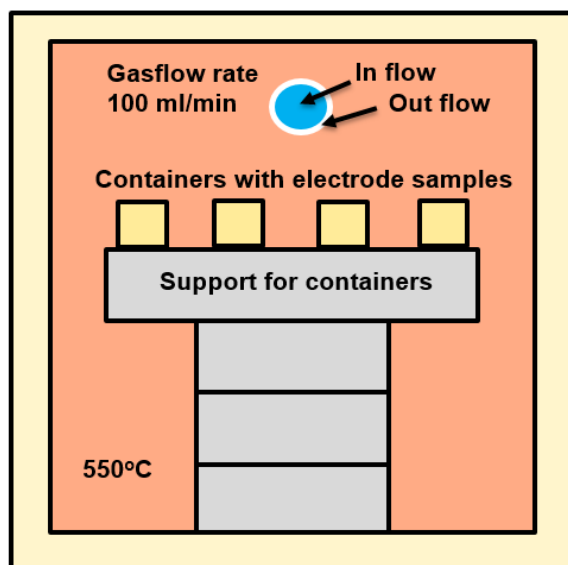


Figure 1: A setup for aging the electrode samples.

A complete fuel cell was fabricated through a co-pressing method. First, composite anode and cathode powders were prepared by mixing GDC/NLC nanocomposite electrolyte with NiO and LSCF, respectively. Polyvinyl-alcohol and ethyl-cellulose were added in the composite electrode powders to increase porosity in the device electrodes. The composition of the nanocomposite electrolyte powder was 70 wt% GDC and 30 wt% NLC. The composition of the electrodes powders was 45 wt% NiO (for anode) or LSCF (for cathode), 45 wt% nanocomposite electrolyte, 5 wt% of Polyvinyl-alcohol and 5 wt% of ethyl-cellulose. The electrode and electrolyte powders were sequentially added in a 13 mm diameter die and then pressed at 250 MPa for 2 minutes. The cell was sintered at 690 °C for 60 minutes with a heating rate of 2 °C/min. Gold paste was applied on both sides of the cells for better electrical contact between the cell and the gold electrode wires.

Characterization

The phase compositions of the powders from the compatibility test were measured with an X-ray diffraction (XRD) unit (PANalytical X'Pert PRO MPD). The powders were further

crushed in a mortar and then measured at room temperature using Cu $K\alpha_1$ radiation (45 kV and 40 mA; $\lambda = 1.5406 \text{ \AA}$). The morphological properties of the powders were also characterized using a transmission electron microscopy (TEM, JEOL JEM-2200FS) equipped with an energy dispersive X-ray detector (EDS).

The electrochemical impedance spectroscopy (EIS) was performed using a Zahner Elektrik's IM6 impedance measurement unit. All of the measurements were conducted at open circuit voltage at 550 °C using an AC signal with an amplitude of 20 mV. A frequency range of 100 mHz to 100 kHz was used to measure the performance of all the symmetric cell samples. In addition, impedance of a LSF symmetric cell was measured using wider frequency ranges (lower limit either 50 μ Hz or 0.2 mHz) in order to reach a deeper understanding of the properties of the electrode. Furthermore, a cyclic voltammetry study was conducted for a LSF symmetric cell using the IM6 unit. This measurement was performed in air between -0.5 V and 0.5 V at a very slow slew rate (300 μ V/s). For all these electrochemical measurements, gold meshes were used as current collectors and the measurement was undertaken using a Probostat measurement setup (NorECs).

Brunauer Emmett-Teller (BET) and Barrett-Joyner-Halenda (BJH) analyses were respectively used to measure the surface area and to estimate the cumulative volume of pores of the sintered composite electrode materials using a liquid nitrogen cooled gas sorption analyser (Micromeritics TriStar 3020) operating at -196 °C. The samples were small pieces of the electrode layer of the symmetric cells. Prior to the measurement, the samples were first dried for 1 hour at 400 °C. The morphological properties of the cells were also studied using a scanning electron microscope (SEM, JEOL JSM-7500FA) coupled with EDS.

3. Results

BET and BJH analysis

Results from BET and BJH experiments are shown in Table 2. Among the composite electrode materials, LSM + NLC was found to have the largest surface area and pore

volume (0.568 m²/g and 4.387 mm³/g). Other composite electrode materials, LSC + NLC, LSF + NLC and LSCF + NLC, were found to have approximately similar surface area and pore volume (0.431 m²/g, 0.428 m²/g, 0.426 m²/g and 2.301 cm³/g, 2.791 cm³/g, 2.217 cm³/g, respectively). However, it was noticed that the porosity of these composite electrodes corresponding to the BJH pore volumes was very low (0.48%, 0.28%, 0.34% and 0.27% respectively). The reason for these low porosity values is that this method takes into account only a certain range of pore sizes in the pore volume estimation. In our case, BJH took into account pore sizes between 1.7 nm and ~300 nm (maximum limit of the equipment) while larger pores were partially ignored. Therefore, we like to highlight that the BJH method is not generally reliable for studying the electrodes of LT-SOFC. However, BET analysis is not largely affected by the pore size distribution and is hence quite reliable.

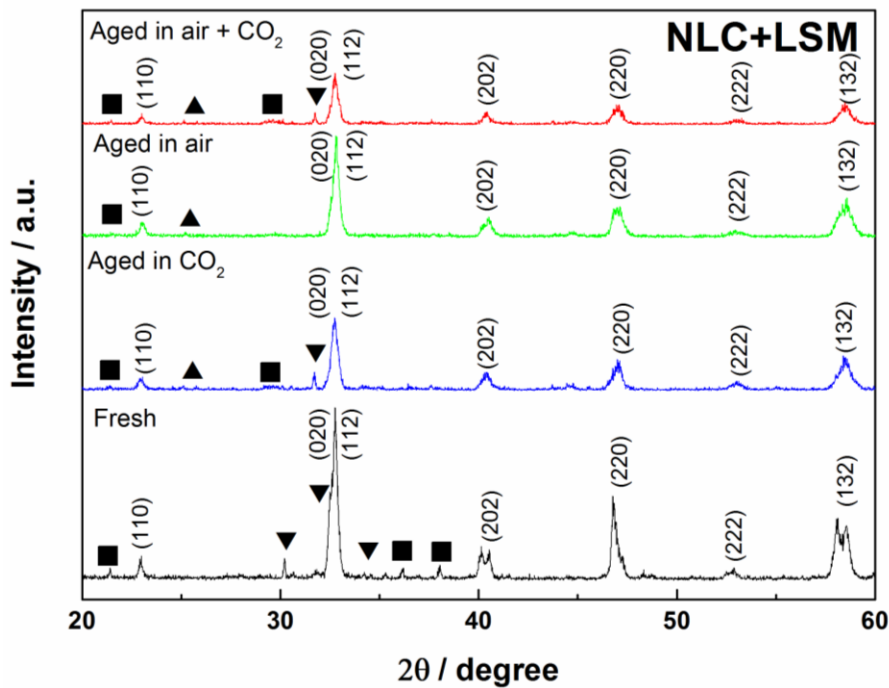
Table 2: The surface area and the pore volume of the electrodes of symmetric cells. The attained porosity value through the BJH method is very low because the method partially ignores large pores in the structure.

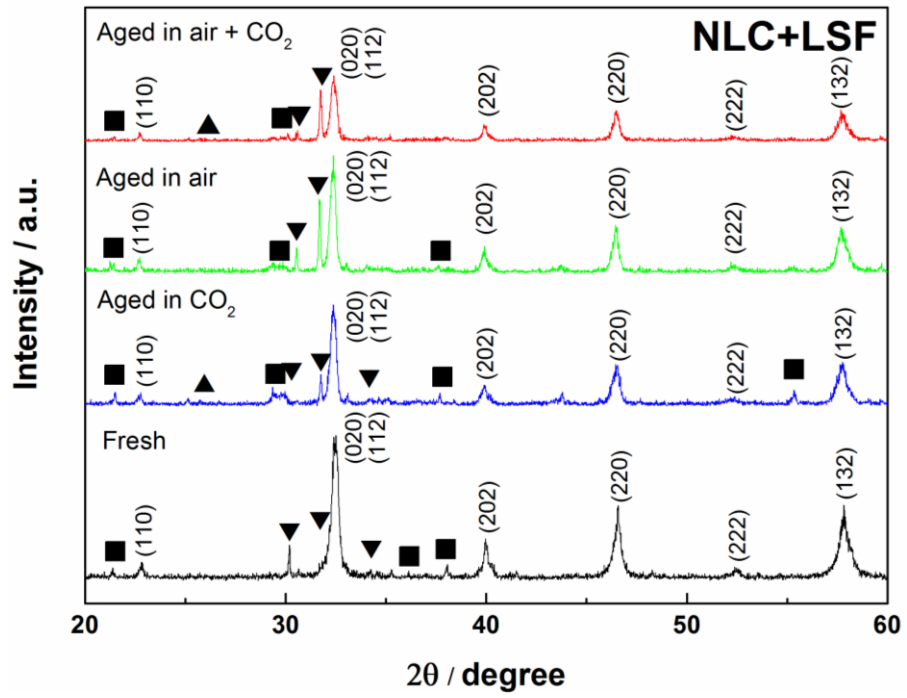
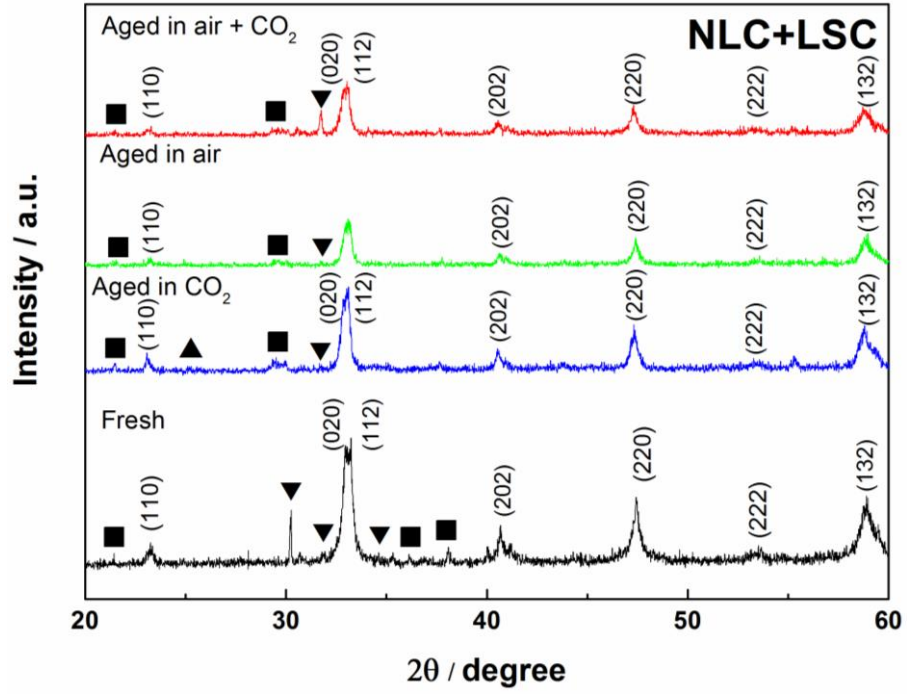
Cathode materials	BET Surface area / m²g⁻¹	BJH pore volume / mm³g⁻¹	Porosity / %
LSM + NLC	0.568	4.387	0.48
LSC + NLC	0.431	2.301	0.28
LSF + NLC	0.428	2.791	0.34
LSCF + NLC	0.426	2.217	0.27

XRD

XRD measurements were conducted on the composite electrode materials before and after the short term compatibility test, and the results are presented in Figure 2. Most of the major peaks corresponded to LSM, LSC, LSF and LSCF, while other major peaks were associated to Li₂CO₃. Several smaller peaks could be attributed to NaLiCO₃ and a small

peak at around 25° was attributed to SrCO_3 as shown in a previous study [15]. However both in our study and in the previous study, the intensity of the SrCO_3 was very low and thus, it remains unclear whether Sr reacts with carbonate or not. Furthermore, all these peaks in the spectra corresponded to those of the perovskite phase or crystallized alkaline carbonates as reported earlier [15]. ICDD patterns corresponding to NaLiCO_3 (021-0954, 84-2168), LiCO_3 (08-0471, 72-1216), LSM (06-9331), LSC (13-6792), LSF (35-1480, 12-5632) and LSCF (89-1268) matched well to the XRD spectra. It was observed that a peak at $\sim 30.2^\circ$ appeared in all fresh electrode powdered samples, however this peak disappeared in most of the samples after the compatibility test. Furthermore, in some cases a new peak appeared at $\sim 31.8^\circ$ after the compatibility test. This peak at $\sim 31.8^\circ$ was most pronounced in case of NLC+LSF sample. Nevertheless, XRD measurements should be performed on all the samples after long term stability test of at least over 100 hours to evaluate their stability in nanocomposite LT-SOFCs.





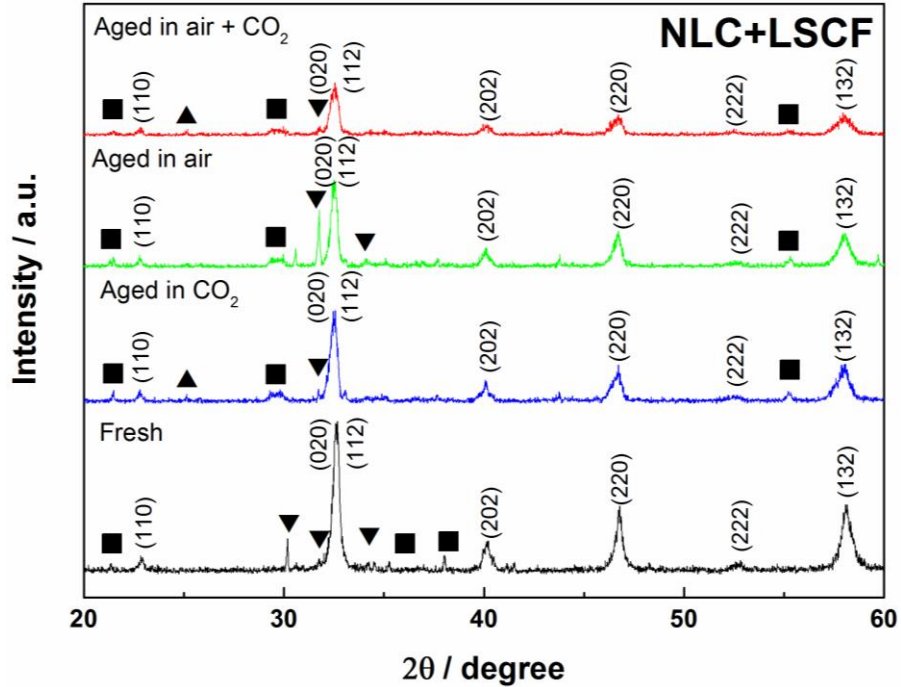
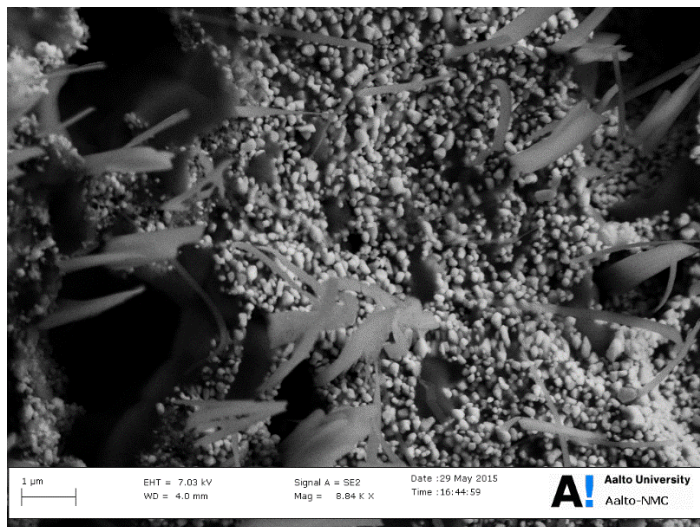


Figure 2: Powder X-ray diffraction patterns of the four nanocomposite electrode materials. Prior to the measurement, the samples were kept in an oven at 550°C for 5 hours under air, CO₂ and air (50 vol%) + CO₂ (50 vol%) atmospheres. The symbols used in the figure represent following materials:

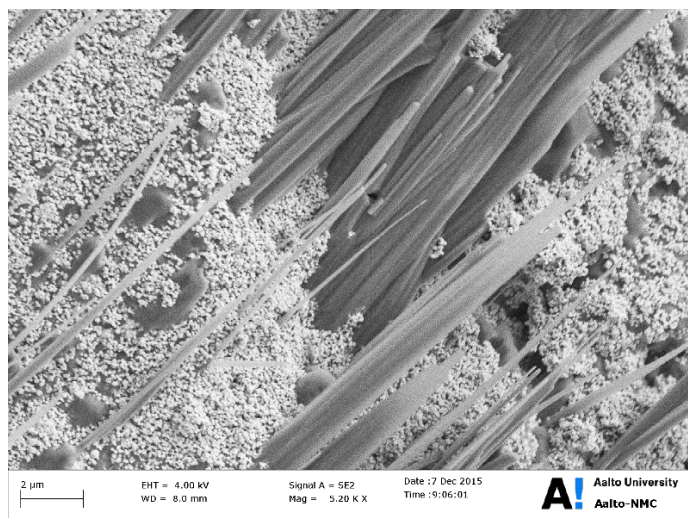
■LiNaCO₃, ▼Li₂CO₃, ▲SrCO₃.

Microstructural and elementary analysis

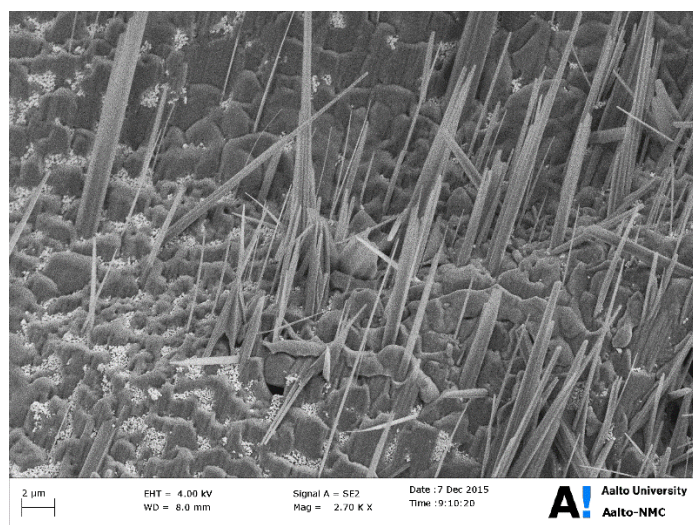
SEM images of symmetric cells with LSM + NLC, LSC + NLC, LSF + NLC and LSCF + NLC are shown in Figure 3. The average particle size in LSM + NLC was approximately 50 nm, whereas in LSC + NLC, LSF + NLC and LSCF + NLC samples, the average particle size was approximately 80 nm.



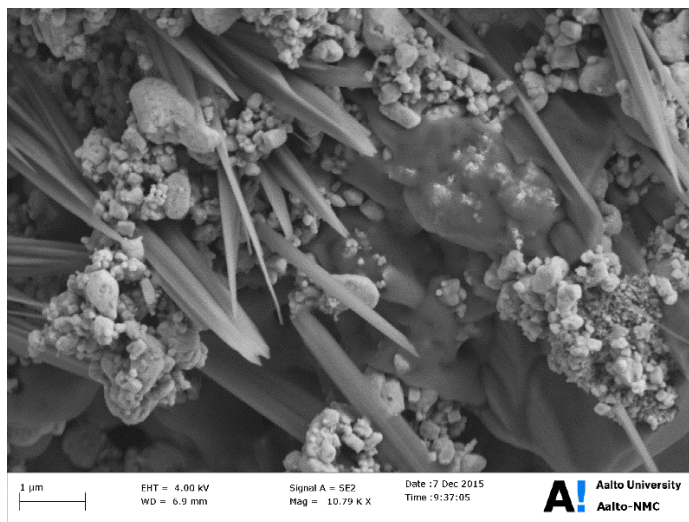
(a)



(b)



(c)



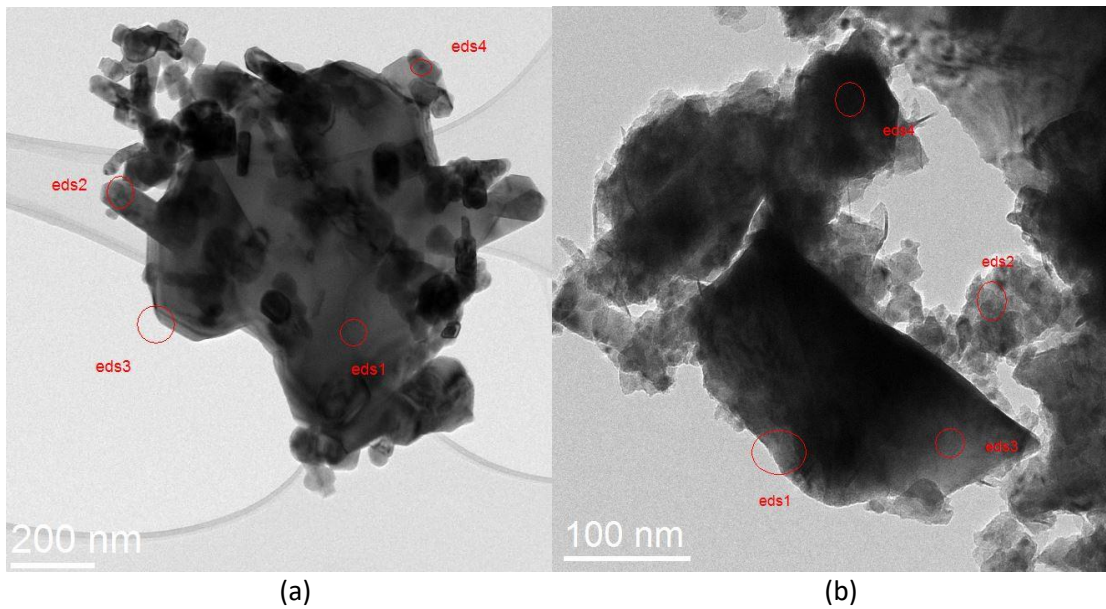
(d)

Figure 3: SEM images of symmetric cells with a) LSM + NLC, b) LSC + NLC, c) LSF + NLC and d) LSCF + NLC.

Furthermore, fibre-shaped structures were found in the SEM images in all of the samples as shown in the Figure 3. It is assumed that these might have been either due to a presence of hydroxides in the samples or a presence of Li_2CO_3 [17]. EDS was performed on LSM + NLC, but, it was not possible to obtain EDS data from the fibre-shaped structures alone due to the following reasons. The EDS signal comes from approximately a micrometer sized volume, although the size of the interaction volume depends (mostly) on the acceleration voltage used in the measurement and the atomic number of studied element. Lithium and the possible hydrogen cannot be detected with EDS due to their small interaction area but all the other elements from LSM + NLC were found in the EDS spectra. Therefore, the cause of the fibre-shaped structures remains inconclusive. A more exact size of the interaction volume could be estimated, for example, by doing some simulations regarding the electron paths in the specimen with a given electron energy and specimen's atomic number.

TEM images of LSM + NLC, LSC + NLC, LSF + NLC and LSCF + NLC powders that were shortly aged under CO_2 atmosphere are shown in Figure 4. EDS elementary analysis was performed to various areas of the samples in order to investigate the structural changes

in the composite electrode materials. EDS spectra of selected areas from Figure 4a are shown in Figure 5. The EDS measurement on aged LSM + NLC sample at the “eds1” area shows all the elements of LSM + NLC except lithium due to the aforementioned reason (Figure 5a). On the other hand, EDS measurement at the “eds4” area revealed higher counts of manganese relative to lanthanum and strontium (Figure 5b). No such behaviour i.e. higher counts of iron or cobalt, was observed for the other aged nanocomposite electrode materials, that is, LSC + NLC, LSF + NLC and LSCF + NLC. Examples of the EDS data from all the samples are shown in the supplementary information. Degradation of LSM due to reaction with molten-carbonates has been previously reported [14]. In this study, higher counts of manganese were observed at only few spots. Furthermore, origin of their cause is not clear. Therefore, it is suggested to perform long term aging of the samples before conducting EDS analysis.



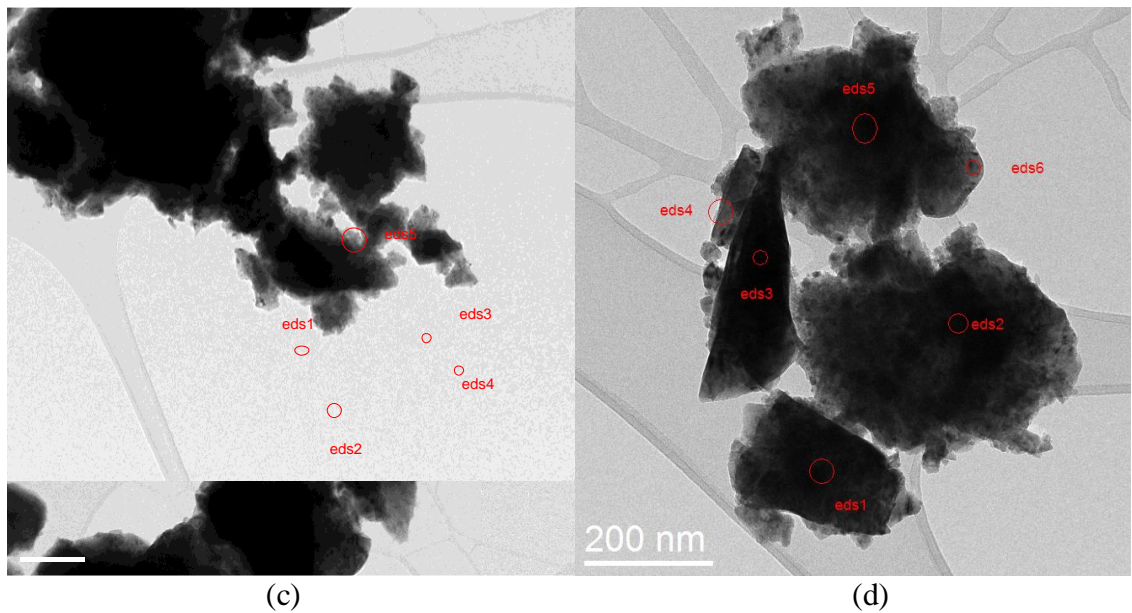
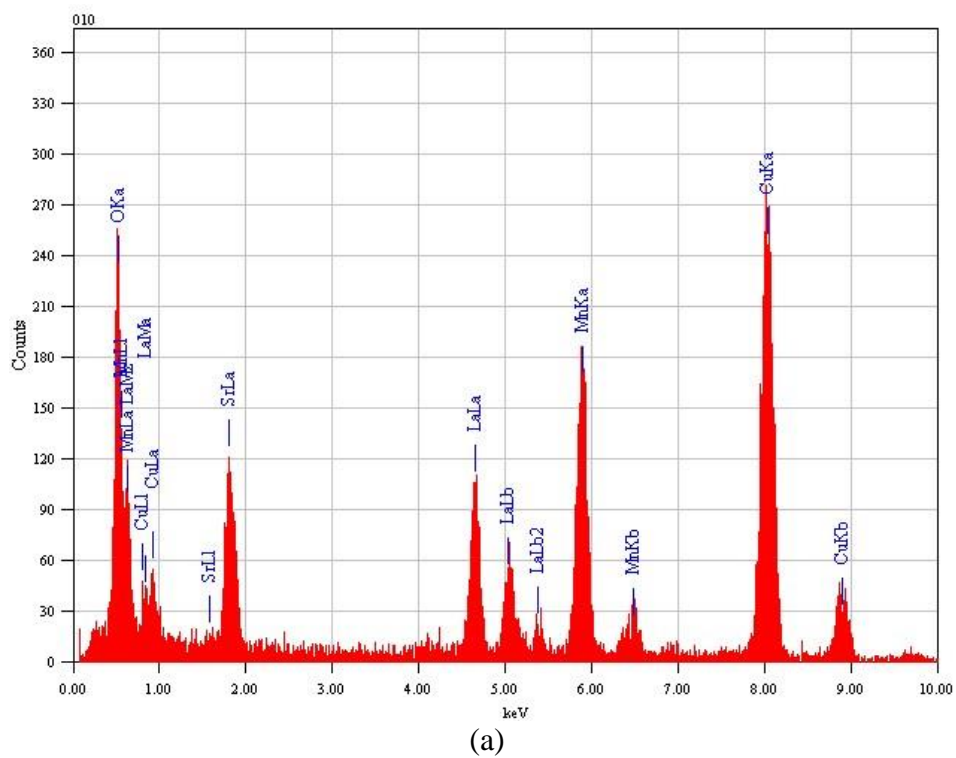


Figure 4: TEM images of a) the LSM + NLC, and b) the LSC + NLC powder, c) the LSF + NLC powder and d) the LSCF + NLC powder, all aged under CO₂ atmosphere at 550°C for 5 hours. EDS was conducted on the marked areas in the images.



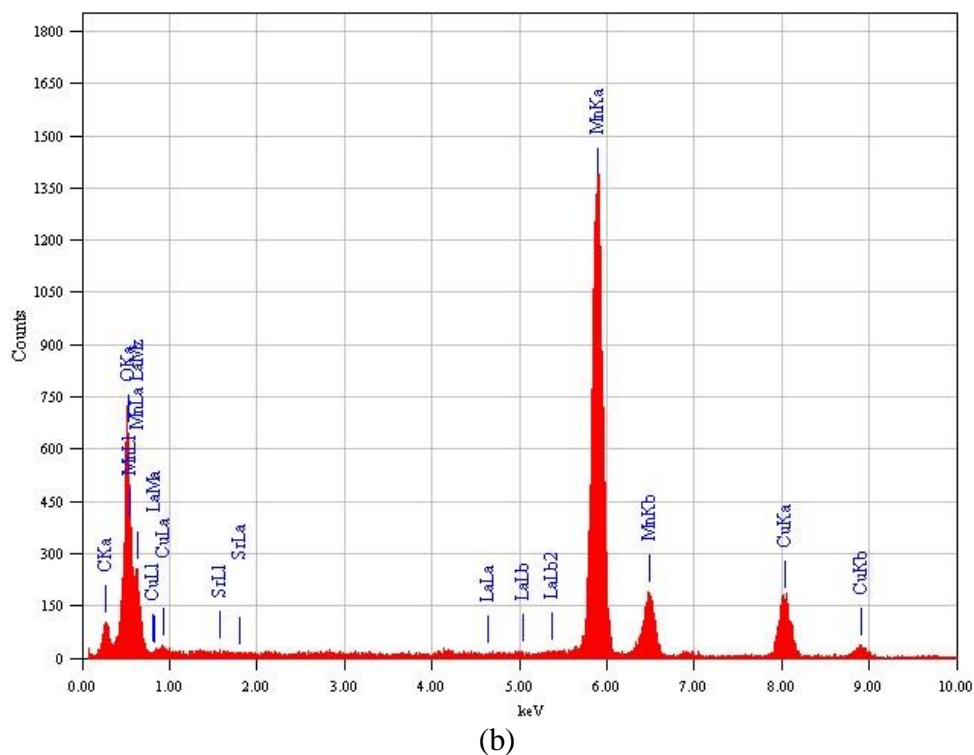


Figure 5: EDS analysis on: a) area marked with “eds1”, b) area marked with “ed4” in aged LSM + NLC sample image shown in Figure 4a.

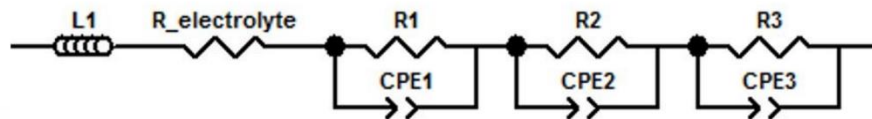
Electrochemical measurements

In this section, results from electrochemical measurements are presented and, for the sake of simplicity, symmetric cells are referred according to their perovskite electrode material. Initially, electrochemical impedance of the symmetric cells were measured at 550 °C in air using a frequency range of 100 mHz to 100 kHz and the corresponding impedance responses of the symmetric cells are shown in Figure 6. The high frequency intercept with the real axis corresponds to the ohmic resistance of a cell, which is primarily dominated by the resistance of the electrolyte. LSC, LSF and LSCF cells produced a typical electrode impedance behavior which consists of three (depressed) semicircles with different time constants, although only a small part of the third (low frequency) semicircle can be seen in the data. The high and intermediate frequency semicircles are often associated to charge transfer reactions while the tail is often associated to the adsorption (dissociative or

associative route) of an oxygen molecule and/or diffusion [29]. On the other hand, LSM showed practically only one highly depressed semicircle. It is assumed, that the same processes are included in the semicircle although they cannot be easily distinguished from each other.

In this work, an equivalent circuit shown in Figure 6a was used to fit the impedance data that was acquired using the frequency range of 100 mHz to 100 kHz. $R_{\text{electrolyte}}$ and $L1$ represent the ohmic resistance and the inductance of the measurement setup, respectively. Two of the R-CPE circuits are assumed to represent the charge transfer processes. On the other hand, the tail is commonly represented with a Warburg element in the literature [14, 30], a third R-CPE element is used here instead due to reasons that are explained later. The fitted data is shown in Figure 7b, and the parameters used to fit the data are shown in Table 3. The high inductances ranging from 0.37 to 0.49 μH were mainly due to long wires used in the measurements. The ohmic resistance, dominated by the resistance of the electrolyte, ranges from 0.78 to 0.99 $\Omega \text{ cm}^2$ which is likely due to small uncontrolled variations in the thickness of the electrolyte layers. $R1$ and $R2$ represent the resistances from the charge transfer reactions whereas $R3$ represents the resistance of the tail i.e. the low frequency semicircle. The combined value for the assumed charge transfer resistance ($R1+R2$) and the resistance associated with the adsorption/diffusion processes ($R3$) was the lowest for LSC (14.12 $\Omega \text{ cm}^2$), followed by LSF (15.23 $\Omega \text{ cm}^2$) and LSCF (19.38 $\Omega \text{ cm}^2$). In case of LSM, the resistances associated with the electrode reactions are significantly higher ($>300 \Omega \text{ cm}^2$) than with the other composite electrode materials. Also, since the electrodes are in series in these symmetric cells, the resistance of the single electrode is half of these values.

a)



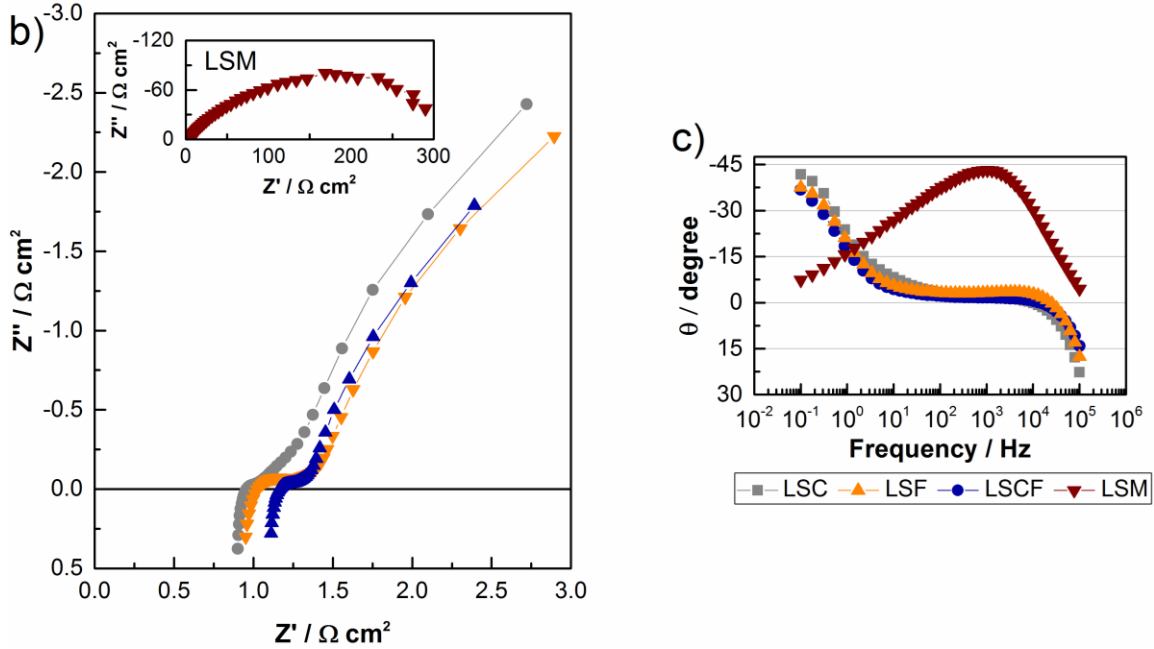


Figure 6: a) An equivalent circuit model, b and c) EIS of all the symmetric cells measured at 550°C in air using a frequency range of 100 mHz to 100 kHz.

Table 3: Resistance values corresponding to electrode reactions using the equivalent circuit shown in Figure 6b and a frequency range of 100 mHz to 100 kHz.

Samples	L1 / μH	R _{electrolyte} / $\Omega \text{ cm}^2$	R1 / $\Omega \text{ cm}^2$	R2 / $\Omega \text{ cm}^2$	R1+R2 / $\Omega \text{ cm}^2$	R3 / $\Omega \text{ cm}^2$	R1+R2+R3 / $\Omega \text{ cm}^2$
LSC	0.49	0.78	0.26	0.25	0.51	13.61	14.12
LSF	0.44	0.82	0.46	0.13	0.59	14.64	15.23
LSCF	0.37	0.99	0.30	0.05	0.35	19.03	19.38

As mentioned earlier, the tail part is usually associated with adsorption/diffusion processes and is often fitted using a Warburg element in the equivalent circuit model [14]. In order to gain a deeper understanding of the electrode behaviour, the impedance of the symmetric LSF cell was measured again using lower frequency limits. In the first additional measurement, the lower frequency limit was 0.2 mHz (Figure 7b) and 50 μHz in the second measurement (Figure 7c). It was found that the tail in Figure 6a exhibited a semicircle behaviour and that an additional semicircle appeared at even lower frequencies. As no Warburg characteristics were seen, an equivalent circuit with four R-CPE circuits (along with R_{electrolyte} and L1) was used (Figure 7a). Fitted parameters from these measurements

are shown in Table 4. Interestingly, it was observed that the total impedance of the LSF decreases to $33.61 \Omega \text{ cm}^2$ after a continues exposure at $550 \text{ }^\circ\text{C}$ for 280 hours from a total initial impedance of 40.38 at $550 \text{ }^\circ\text{C}$. It is also important to note that the resistances represented by R1, R2 and R3 originated from both sides of the cell. Thus, the resistances for a single electrode is half of the presented values.

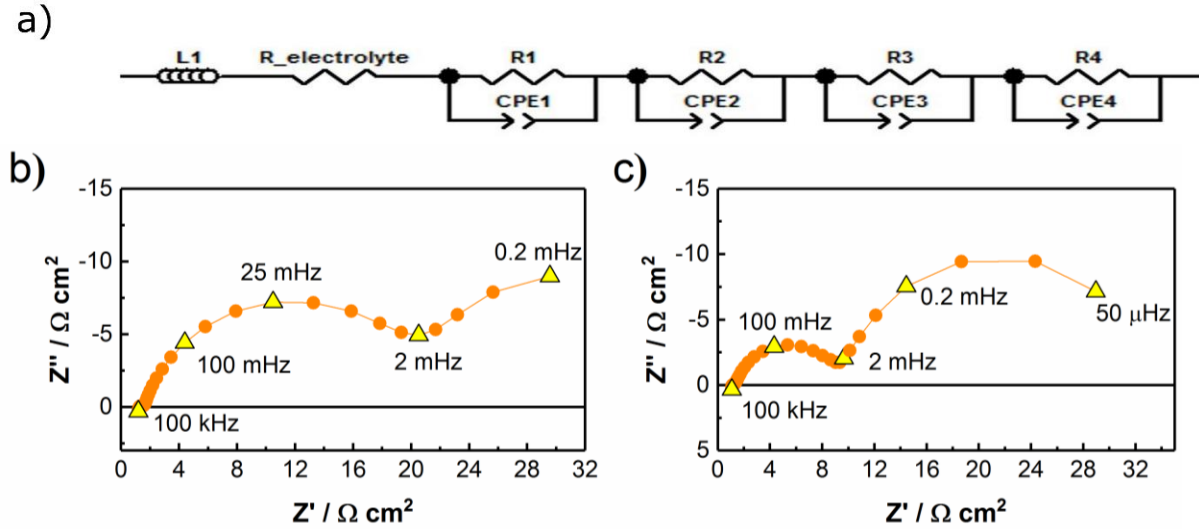


Figure 7: a) An equivalent circuit used to fit the data corresponding to low frequency measurements. Impedance data of the LSF cell measured at $550 \text{ }^\circ\text{C}$ in air, using a frequency range of b) $0.2 \text{ mHz} - 100 \text{ kHz}$ (after ageing the cell for 24 hours at $550 \text{ }^\circ\text{C}$) and c) $50 \mu\text{Hz} - 100 \text{ kHz}$ (after ageing the cell for 280 hours at $550 \text{ }^\circ\text{C}$).

Table 4: Resistance values corresponding to electrode reactions of LSF cell shown in Figure 7 b and c using the equivalent circuit. Exposure time of the LSF cell in air at 550°C is mentioned to clarify that the same LSF sample is used in all these measurements and it refers to the total time cell has been exposed to the test condition.

Frequency range	Exposure time in air at $550 \text{ }^\circ\text{C}$	R_electrolyte / $\Omega \text{ cm}^2$	R1 / $\Omega \text{ cm}^2$	R2 / $\Omega \text{ cm}^2$	R1+R2 / $\Omega \text{ cm}^2$	R3 / $\Omega \text{ cm}^2$	R4 / $\Omega \text{ cm}^2$	Sum of the resistances / $\Omega \text{ cm}^2$
-----------------	--	---------------------------------------	----------------------------	----------------------------	-------------------------------	----------------------------	----------------------------	--

100 mHz – 100 kHz	0 hours	0.82	0.46	0.13	0.59	14.64	-	-
0.2 mHz – 100 kHz	2 hours	1.00	0.52	0.08	0.60	18.67	19.51	40.38
Cyclic voltammetry studies	200 hours	-	-	-	-	-	-	39.45 (IV from Figure 8)
50 μ Hz – 100 kHz	280 hours	0.87	0.44	0.09	0.53	8.08	23.13	33.14

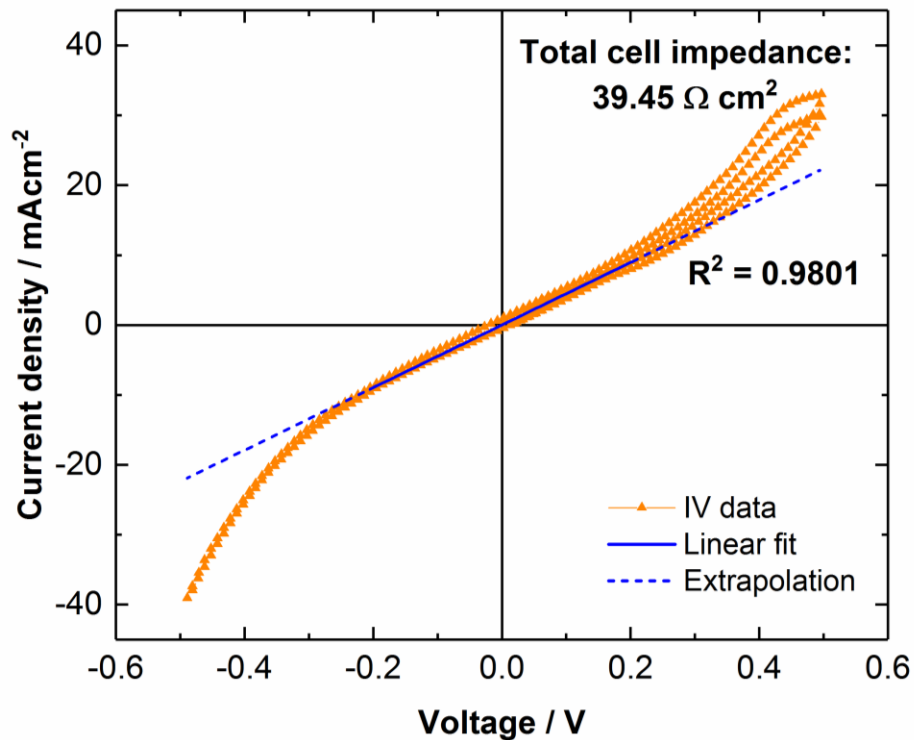


Figure 8: A cyclic voltammetry measurement for a LSF cell.

The total impedance of a LSF cell was also attained using a cyclic voltammetry measurement and the results are shown in Figure 8. As the impedance measurements were conducted at open circuit voltage (~ 0 V), the slope of the current-voltage curve at around 0 V could be used for measuring the total resistance of the cell for comparison. The first objective of this measurement was also to test the linearity of the current-voltage curve,

since impedance data has been measured using AC amplitudes as high as 500 mV [14,15,31]. As the current-voltage curve in Figure 9 is not linear above 200 mV, it is not recommended to use higher amplitudes than 200 mV in EIS measurements. The second objective was to confirm that the EIS measurements ranged to sufficiently low frequencies to bring all significant resistance components visible in the EIS spectrum. The total resistance of the LSF cell (calculated from the slope of the current-voltage curve) was 29.73 Ω and the respective area specific resistance was 39.45 Ω cm². This matches almost exactly with the total resistance attained in the EIS measurement (0.2 mHz – 100 kHz) which was 40.84 Ω cm² (Table 4). This result, together with the fact that the EIS amplitude was within the linear region, confirms that no additional major impedance components exist outside the measured frequency range below 50 μ Hz. Thus, the EIS data fully characterizes the total DC resistance of the sample. For this reason, we recommend to do a quantitative comparison of the low-frequency limit of the EIS data (and the fitted equivalent circuit) against the slow-sweep rate cyclic current-voltage data. This comparison is useful for all studies where the DC resistance of sample is an important property of the sample, such as for experiments on SOFC electrode/electrolyte materials. We note that the significant low-frequency impedance component in Figure 8 would have been missed if the EIS had been taken only down to 1 Hz which is a typical lower limit of frequencies reported in similar studies [14,15,32,33]. The slow sweep-rate cyclic voltammetry measurement, which in the present case took as long as 38 hours to complete, is also an undisputable way to confirm and show the electrochemical stability of the sample at the used measurements conditions.

Next, characterization of a complete fuel cell using nanocomposite electrolyte and its composites with NiO and LSCF as anode and cathode, respectively, is presented. The composition of the composite anode was 45 wt% NiO, 45 wt% nanocomposite electrolyte, 5 wt% polyvinyl-alcohol and 5 wt% ethyl-cellulose. Similarly, the composition of composite cathode was 45 wt% LSCF, 45 wt% nanocomposite electrolyte, 5 wt% polyvinyl-alcohol and 5 wt% ethyl-cellulose. Polyvinyl-alcohol and ethyl-cellulose were added in the composite electrodes to increase the surface area for efficient reaction kinetics

at the electrodes. The surface areas of the nanocomposite anode and cathode were measured using BET analysis and found to be 2.831 m²/g and 2.679 m²/g, respectively. The electrochemical characterization of this cell is presented in the following section.

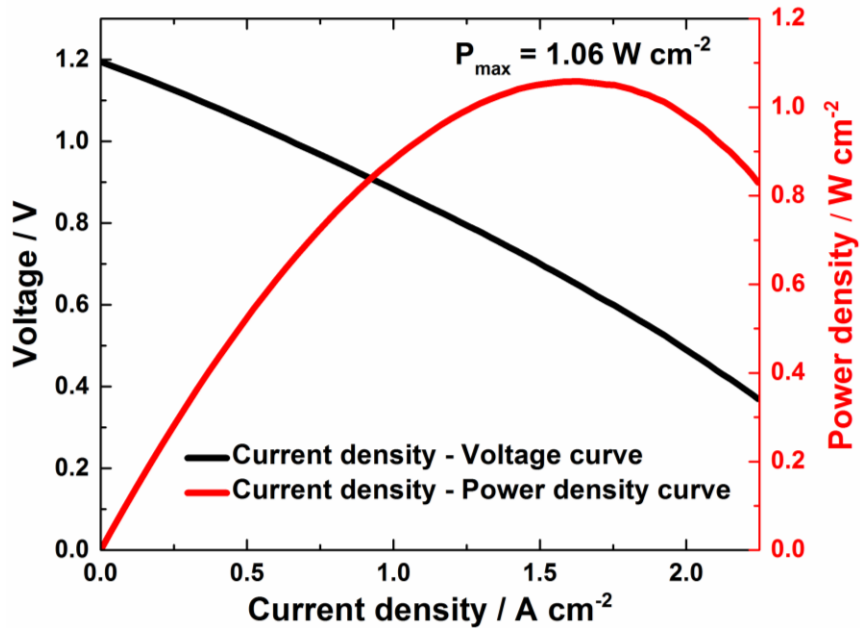
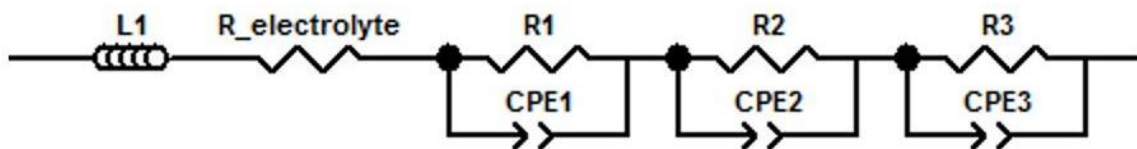
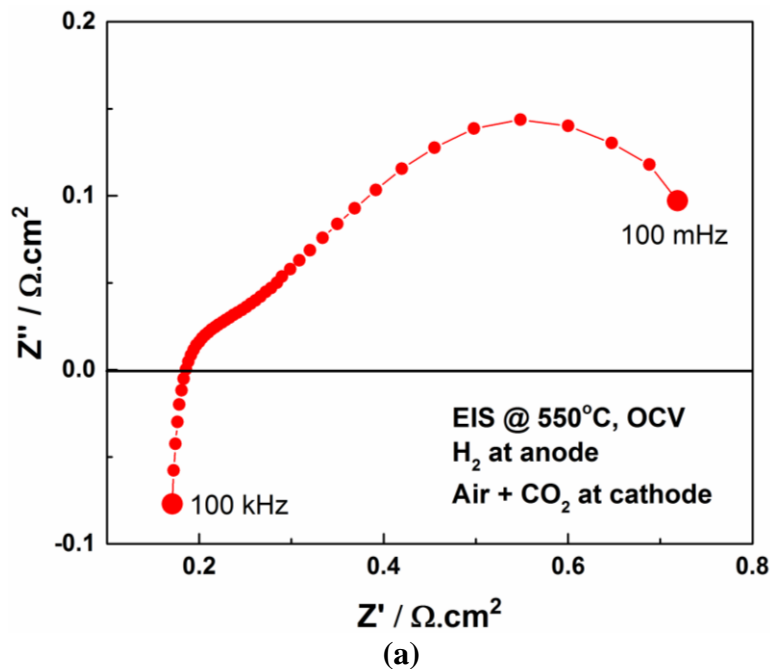


Figure 9: Cell voltage and power density versus current density under operating conditions, H₂ at anode and air + CO₂ at cathode, at 550°C.

The nanocomposite fuel cell produced an output power density of 1.06 W/cm² at 550°C as shown in Figure 9. The cell exhibits an open-circuit voltage (OCV) of ~1.19 V. The total resistance of the cell obtained through IV curve at maximum power point was 0.40 Ω cm². This high performance of the cells demonstrates the efficient ion transport and reactions kinetics in the cells. To understand the processes in the cell, the EIS was performed on the same cell at open cell circuit condition as shown in Figure 10a and the EIS spectra of

the cell were fitted to an equivalent circuit model shown in Figure 10b. $R_{\text{electrolyte}}$ and $L1$ represent the ohmic resistance and the inductance of the measurement setup, respectively. Three pair of R-CPE circuits are used to fit the two distinguished semicircles and an intermediate region between them. Generally in these fuel cells, the reaction kinetics is much faster at the anode as compared to the cathode [34] which gives an indication that the time constant of the reaction processes at anode should be lower than the time constant of reaction processes at cathode. The first R-CPE represents the impedance to the charge transfer reactions in the cell. The second and third R-CPE elements were fit to the intermediate region and the low frequency semicircle, which represent the impedance related to the processes related to mass transfer such as gas diffusion in porous structure, gas solubility into molten phase and gas diffusion through electrolyte membrane [35,36].



(b)

Figure 10: a) EIS response of the cell measured at 550°C using a frequency range of 100 mHz to 100 kHz, and b) An equivalent circuit model to fit the EIS response of the cell.

The parameters used to fit the data and their values are shown in Table 5. The high inductance 0.57 μH was mainly due to long wires used in the measurements. The ohmic resistance, dominated by the resistance of the electrolyte, was 0.18 $\Omega \text{ cm}^2$. R1 represents the resistances from the charge transfer reactions (0.15 $\Omega \text{ cm}^2$), whereas R2 and R3 represent the resistances from the mass-transfer processes (0.13 $\Omega \text{ cm}^2$ and 0.44 $\Omega \text{ cm}^2$).

Table 5: Resistance values corresponding to fuel cell processes using the equivalent circuit shown in Figure 10b.

L1	R_electrolyte	R1	R2	R3
/ μH	/ $\Omega \text{ cm}^2$			
0.57	0.18	0.15	0.13	0.44

4. Conclusions

Short-term compatibility tests were performed for LSM, LSC, LSF and LSCF materials at 550 °C under air, CO₂ and air/CO₂ atmospheres. On the basis of XRD, TEM and EDS analysis, it was concluded that LSM is not suitable for these ceramic-carbonate composite fuel cells. Long term test of at least over 100 hours should be performed to evaluate their stabilities for nanocomposite LT-SOFC. The EIS measurements showed that LSC, LSF and LSCF have significantly lower resistance to oxygen reduction reaction (14.12 $\Omega \text{ cm}^2$, 15.23 $\Omega \text{ cm}^2$ and 19.38 $\Omega \text{ cm}^2$ respectively), compared to LSM (>300 $\Omega \text{ cm}^2$). As opposed to the current knowledge in the literature, low frequency measurements down to 50 μHz

were necessary to reveal two additional significant semi-circles at frequencies below about 1 Hz. These semicircles can yield additional information about the electrochemical reactions important for full performance characterization of LT-SOFC materials. Both low frequency EIS and steady state current voltage measurements are thus recommended to be undertaken for characterising all the electrode processes, especially those seen only at very low frequencies. Nanocomposite fuel cell demonstrated an outstanding performance of 1.06 W/cm² at 550°C taking advantage of the composite effect to boost the ionic transport in the electrolyte layer and efficient reaction kinetics at the electrodes.

Acknowledgements

This work is a part of EU-Indigo project. The authors especially thank Academy of Finland for their financial support (Grant No. 13282962 and 13297204) with the framework of EU New Indigo programme. This work made use of the premises from Aalto University Nanomicroscopy Center (Aalto-NMC), Laboratory of Inorganic Chemistry and Department of Forest Products Technology.

References

- [1] Rajesh S, Maccedo DA, Nascimento RM. Materials and processes for energy: communicating current research and technological developments. Formatex Research Center, 2013, 485-494.
- [2] Park SY, Ahn JH, Jeong CW, Na CW, Song RH, Lee JH. Ni-YSZ-supported tubular solid oxide fuel cells with GDC interlayer between YSZ electrolyte and LSCF cathode. International Journal of Hydrogen Energy, 2014, 39: 12894-12903.
- [3] Kakac S, Pramuanjaroenkij A, Zhou XY. A review of numerical modelling of solid oxide fuel cells. International Journal of Hydrogen Energy, 2007, 32: 761-786.
- [4] Ho TX, Kosinski P, Hoffmann AC, Vik A. Effects of heat sources on the performance of a planar solid oxide fuel cell. International Journal of Hydrogen Energy, 2010, 35: 4276-4284.

- [5] Asghar MI, Lund PD. Improving catalyst stability in nano-structured solar and fuel cells. *Catalysis Today*, 2015, 259, 259-265.
- [6] Yokokawa H, Tu H, Iwanschitz B, Mai A. Fundamental mechanisms limiting solid oxide fuel cell durability. *Journal of Power Sources*, 2008, 182: 400-412.
- [7] O'Hayre R, Cha SW, Colella W, Prinz FB. *Fuel cell fundamentals*. Wiley, 2006, 245-246.
- [8] Patakangas J, Ma Y, Jing Y, Lund P. Review and analysis of characterization methods and ionic conductivities for low-temperature fuel cells (LT-SOFC). *Journal of Power Sources*, 2014, 263: 315-331.
- [9] Fergus JW. Electrolytes for solid oxide fuel cells. *Journal of Power Sources*, 2006, 162: 30-40.
- [10] Ivers-Tiffée E, Weber A, Herbstritt D. Materials and technologies for SOFC-components. *Journal of the European Ceramic Society*, 2001, 21: 1805-1811.
- [11] Kilner JA, Burriel M. Materials for Intermediate-Temperature Solid-Oxide Fuel Cells. *Annual Review of Material Research*, 2014, 44: 365-393.
- [12] Jeffrey F, Rob H, Xianguo L, David PW, JiuJun Z. *Solid Oxide Fuel Cells: Material Properties and Performance*. Chemical Rubber Company Press, 2009, 33-37.
- [13] Lee JG, Park JH, Shul YG. Tailoring gadolinium-doped ceria-based solid oxide fuel cells to achieve 2 Wcm^{-2} at $550 \text{ }^\circ\text{C}$. *Nature Communications*, 2014, 5: 4045.
- [14] Pereira JRS, Rajesh S, Figueiredo FML, Marques FMB. Composite electrodes for ceria-carbonate intermediate temperature electrolytes. *Electrochimica Acta*, 2013, 90: 71-79.
- [15] Rajesh S, Pereira JRS, Figueiredo FML, Marques FMB. Performance of Carbonate - LaCoO_3 and $\text{La}_{0.8}\text{Sr}_{0.2}\text{Co}_{0.2}\text{Fe}_{0.8}\text{O}_3$ -Composite Cathodes under Carbon Dioxide. *Electrochimica Acta*, 2014, 125: 435-442.
- [16] Loureiro FJA, Rajesh S, Figueiredo FML, Marques FMB. Stability of metal oxides against Li/Na carbonates in composite electrolytes. *Royal Society of Chemistry Advances*, 2014, 4: 59943-59952.
- [17] Chockalingam R, Jain S, Basu S. Studies on Conductivity of Composite GdCeO_2 -Carbonate Electrolytes for Low Temperature Solid Oxide Fuel Cells. *Integrated Ferroelectrics*, 2010, 116: 23-34.

- [18] Tan W, Fan L, Raza R, Khan MA, Zhu B. Studies of modified lithiated NiO cathode for low temperature solid oxide fuel cell with ceria-carbonate composite electrolyte. *International Journal of Hydrogen Energy*, 2013, 38: 370-376.
- [19] Di J, Chen M, Wang C, Zheng J, Fan L, Zhu B. Samarium doped ceria-(Li/Na) 2CO_3 composite electrolyte and its electrochemical properties in low temperature solid oxide fuel cell. *Journal of Power Sources*, 2010, 195: 4695-4699.
- [20] Richter J, Holtappelsm P, Graule T, Nakamura T, Gauckler LJ. Materials design for perovskite SOFC cathodes. *Monatshefte für Chemie*, 2009, 140: 985-999.
- [21] Ota K, Mitsushima S, Kato S, Asano S, Yoshitake H, Kamiya N. Solubilities of Nickel Oxide in Molten Carbonate. *Journal of the Electrochemical Society*, 1992; 139: 667-671.
- [22] Doyon J, Gilbert T, Davies G, Paetsch L. NiO solubility in mixed Alkali/Alkaline Earth Carbonates. *Journal of the Electrochemical Society*, 1987, 134: 3035-3038.
- [23] Jiang SP. A comparison of O₂ reduction reactions on porous (La, Sr)MnO₃ and (La,Sr)(Co,Fe)O₃ electrodes. *Solid State Ionics*, 2002, 146: 1-22.
- [24] Petric A, Huang P, Tietz F. Evaluation of La-Sr-Co-Fe-O perovskites for solid oxide fuel cells and gas separation membranes. *Solid State Ionics*, 2002, 135: 719-725.
- [25] Haile SM. Fuel cell materials and components. *Acta Materialia*, 2003, 51:5981-6000.
- [26] Teraoka Y, Nobunaga T, Okamoto K, Miura N, Yamazoe N. Influence of constituent metal cations in substituted LaCoO₃ on mixed conductivity and oxygen permeability. *Solid State Ionics*, 1991, 48: 207-212.
- [27] Wiemhofer HD, Bregues HG, Nigge U, Zipprich W. *Solid State Ionics*. Studies of ionic transport and oxygen exchange on oxide materials for electrochemical gas sensors. *Solid State Ionics*, 2002, 150: 63-77.
- [28] Seo ESM, Yoshito WK, Ussui V, Lazar DRR, Castanho SRHM, Paschoal JOA. Influence of the starting materials on performance of high temperature oxide fuel cells devices. *Material Research*, 2004, 7: 215-220.
- [29] Adler SB. Factors governing oxygen reduction in solid oxide fuel cell cathodes. *Chemical Reviews*, 2004, 104: 4791-4843.
- [30] Fu Y, Poizeau S, Bertei A, Qi C, Mohanram A, Pietras JD, Bazant MZ. Heterogeneous electrocatalysis in porous cathodes of solid oxide fuel cells. *Electrochimica Acta*, 2015, 159: 71-80.

- [31] Maguire E, Gharbage B, Margues FMB, Labrincha JA. Cathode materials for intermediate temperature SOFCs. *Solid State Ionics*, 2000, 127: 329-335.
- [32] Evans A, Martynczuk J, Stender D, Schneider CW, Lippert T, Prestat M. Low-temperature micro-solid oxide fuel cells with partially amorphous $\text{La}_{0.6}\text{Sr}_{0.4}\text{CoO}_{3-\sigma}$ cathodes. *Advanced Energy Materials*, 2015, 5: 1400747.
- [33] Evans A, Karalic S, Martynczuk J, Prestat M, Tolke R, Yang Z, Gauckler LJ. $\text{La}_{0.6}\text{Sr}_{0.4}\text{CoO}_{3-\sigma}$ Thin films prepared by pulsed laser deposition as cathodes for micro-solid oxide fuel cells. *ECS Transactions*, 2012, 45: 333-336.
- [34] Gao Z, Mogni LV, Miller EC, Railsback JG, Barnett SA. A perspective on low-temperature solid oxide fuel cells. *Energy and Environmental Science*, 2016, 9: 1602-1644.
- [35] Lee C. Analysis of impedance in a molten carbonate fuel cell. *Journal Electroanalytical Chemistry*, 2016; 776: 162–169.
- [36] Nguyen HVP, Kang MG, Ham HC, Choi SH, Han J, Nam SW, Hong SA, Yoon SP. A New Cathode for Reduced-Temperature Molten Carbonate Fuel Cells. *Journal of the Electrochemical Society*, 2014, 161: F1458–F1467.